JOURNAL OF OPTOELECTRONICS AND ADVANCED MATERIALS Vol. 10, No. 3, March 2008, p. 528 - 532

# Photoluminescence processes in $Er^{3+}$-doped Calcium Niobium Gallium Garnet (CNGG) crystals

S. POLOSAN[a,b], K. SHIMAMURA[c], T. TSUBOI[a]

[a]*Faculty of Engineering, Kyoto Sangyo University, Kyoto 603-8555, Japan*

[b]*National Institute of Materials Physics, Bucharest-Magurele, PO Box MG-7, 077125, Romania*

[c]*Optronic Materials Center, National Institute for Materials Science, Tsukuba 305-0044, Japan*

Photoluminescence properties of $Er^{3+}$-doped calcium niobium gallium garnet (CNGG) disordered crystals have been studied in the range of 200-2000 nm at 10-290 K. In addition to emission bands due to $Er^{3+}$, a broad emission band is observed at 470 nm. From the emission spectra that were obtained by various excitations, level assignment has been established for the emission bands. Different temperature dependences are observed between the emission bands at 522 and 543 nm. This is explained using non-radiative phonon relaxation between the $^2H_{11/2}$ and $^4S_{3/2}$ states. Besides the 1535 nm $Er^{3+}$ emission band, near infrared emission bands are observed at 860 and 1240 nm, which are attributed to the transitions from the $^4S_{3/2}$ state to the $^4I_{13/2}$ and $^4I_{11/2}$ states, respectively.

(Received February 28, 2008; accepted March 12, 2008)

*Keywords:* Photoluminescence, CNGG disordered crystal, near infrared emission, non-radiative transition

## 1. Introduction

Rare-earth-doped crystal and glasses are widely used as scintillator [1], solid state lasers, optical communication fibers (especially those doped with $Er^{3+}$ ions [2, 3]), fluoerescent lamps, and cathode ray tubes [4]. Besides their laser-active properties of $Er^{3+}$-doped crystals, these compounds are also used as infrared-to-visible up-convertors [5,6].

Calcium niobium gallium garnet $Ca_3(NbGa)_{2-x}Ga_3O_{12}$ (called CNGG) crystal is particularly of interest because of their disordered structure [7] which gives the possibility of the dopant ions to occupy different positions in the matrix. CNGG crystal is also important for the applications in non-linear optical materials.

Shimamura et al. studied on the rare-earth-doped CNGG crystals, especially its growth process [7], crystal structure [8] and optical properties [9]. The CNGG crystals were also doped with other trivalent ions like $Cr^{3+}$ to study the luminescence from $Cr^{3+}$ ions in CNGG [10]. It was observed that $Cr^{3+}$-doped CNGG shows a strong quenching above room temperature.

Of CNGG crystals doped with various rare earth ions, $Er^{3+}$-doped CNGG crystals have not been studied in detail. The present work was undertaken to clarify the photoluminescence processes in visible and near infrared emission bands due to $Er^{3+}$ ions. The optical properties were measured at not only the room temperature but also low temperatures like 10 K.

## 2. Experimental procedure

$Er^{3+}$-doped CNGG crystals were grown by the Czochralski method using a standard rf-heating furnace and iridium crucible. The raw material consists of a mixture of $CaCO_3$, $Nb_2O_5$ and $Ga_2O_3$ with ratio of 36.472 : 242.36 : 36.286 (wt %) and the dopant powder of $Er_2O_3$. The concentration of $Er_2O_3$. was 3.04 wt %. During the crystal growth, a mixture of inert gases of $O_2$ and $N_2$ was used to avoid the evaporation of gallium oxides from the melt. The grown crystal crystal with a size of 60 mm length and 15 mm diameter was cut to a size of 10x5x1 mm for the spectroscopic measurements.

Absorption and magnetic circular dichroism (MCD) spectra were measured with a Cary 5E spectrophotometer and a Jasco J-40A polarimeter, respectively. Luminescence spectra were measured with a Spex Fluorolog-3 spectrophotometer which contains a 450 W Xe-lamp as an excitation light source. The infrared emission was detected using a Jobin-Yvon

DSSX-IGA010L InGaAs photodiode with sensitivity at 800-1700 nm. The Fluorolog-3 spectrophotometer consists of two monochromators. One is used for excitation of crystal, the other is used for detection of photoluminescence. The slits of excitation and emission monochromators were fixed at 5 nm and 0.2 nm, respectively, for the sharp $Er^{3+}$ luminescence measurement, while at 2 nm and 1 nm for the measurement of broad emission band. Absorption and photoluminescence spectra were investigated at various temperatures between 10 and 300 K in the spectral region 200-2000 nm.

### 3. Experimental results

Figure 1 shows the absorption spectra of $Er^{3+}$-doped CNGG crystals at 12 K and room temperature. The spectra consist of sharp lines at 300-1600 nm and broad band at 325 nm. A sharp rise due to the CNGG host crystal appears at about 245 nm. The intensity of the 325 nm broad band is almost temperature independent. Two absorption bands appear at about 965 nm and 1500 nm in the near infrared region, which are due to the $^4I_{13/2} \rightarrow {}^4I_{11/2}$ and $^4I_{15/2} \rightarrow {}^4I_{11/2}$ transitions in $Er^{3+}$, respectively. No other infrared absorption band was observed at 800-3100 nm.

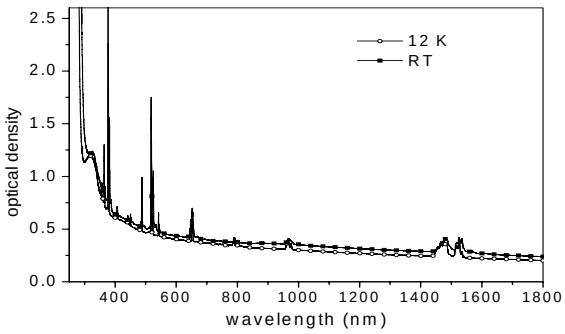


*Fig. 1. Absorption spectra of Er:CNGG at 12 and 290 K.*

Photo-excitation into the visible absorption bands at 543 nm and 667 nm gives different near infrared emission spectra. Excitation at 543 nm gives emission lines at 860, 980, 1012, 1025, 1240 and 1535 nm, while excitation at 667 nm gives only two emission lines at 980 and 1535 nm as shown in Fig. 2. This is confirmed from the excitation spectra for these near infrared emissions as shown in Fig. 3.

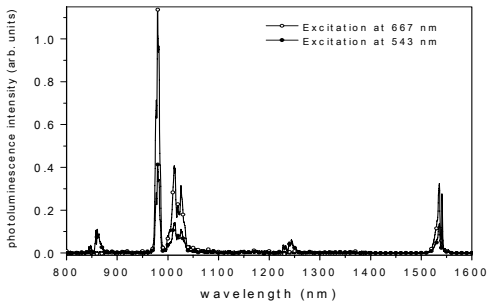


*Fig. 2. Near infrared photoluminescence spectra of Er:CNGG at 12 K. The spectra at 800-1400 nm were enlarged by ten times.*

From comparison with the absorption spectra, the 980, 1012 and 1025 nm lines are attributed to the transition $^4I_{11/2} \rightarrow {}^4I_{15/2}$, while the 1535 nm to the transition $^4I_{13/2} \rightarrow {}^4I_{15/2}$,.

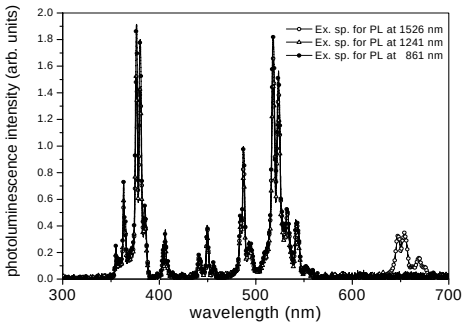


*Fig. 3. Excitation spectra for near infrared emissions at 290 K.*

Figure 4 shows the emission spectrum obtained by excitation at 376 nm at room temperature, which is compared with the absorption spectrum. Unlike the absorption spectrum, emission bands at 519 and 524 nm, which are due to the transition $^2H_{11/2} \rightarrow {}^4I_{15/2}$, is much weaker than the emission bands at 540-565 nm, which are due to the transition $^4S_{3/2} \rightarrow {}^4I_{15/2}$. When temperature is decreased from 290 K to 12 K, the emission bands at 540-565 nm increase but the emission bands at 515-538 nm decrease. The latter bands disappear below 100 K (Fig. 5). The increase of the 540-565 nm band intensity stops below about 100 K and no intensity change is observed below 100 K. These results indicate depopulation of the $^2H_{11/2}$ state and population enhancement of the $^4S_{3/2}$ state with decreasing temperature.

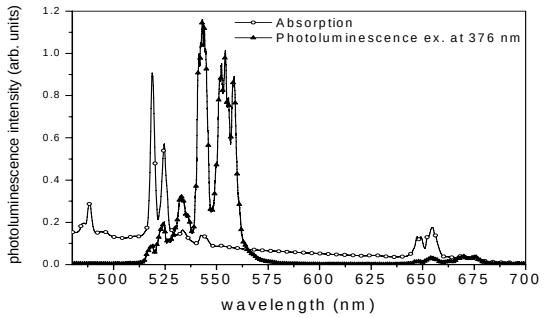


*Fig. 4. Photoluminescence spectrum which was obtained by excitation at 376 nm at 290 K, compared with absorption spectrum.*

Excitation into the band-to-band gap of CNGG host at 280 nm gives a broad emission band with peak at 470 nm at low temperature such as 12 K. This emission band overlaps with the absorption lines due to $Er^{3+}$. Therefore the absorption due to $Er^{3+}$ is observed in the 470 nm emission band as several sharp dips (Fig. 6). The excitation band for the 470 nm emission has a peak at 278 nm.

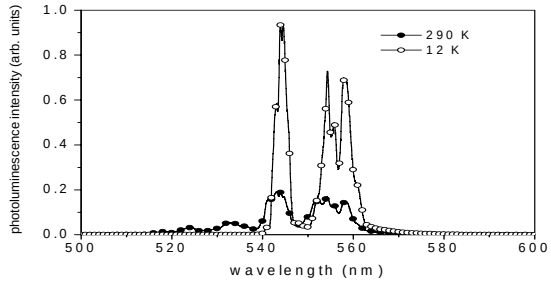


*Fig 5. Photoluminescence spectra of Er:CNGG excited at 376 nm at 12 at 290 K.*

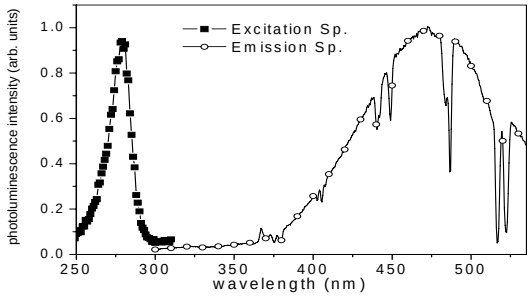


*Fig. 6 Broad blue emission band spectrum of Er:CNGG excited at 280 nm at 12 K, and excitation spectrum for 470 nm emission.*

Fig. 7 shows the MCD spectrum at 290 K and 12 K, together with the absorption spectrum at 290 K. The MCD signal is enhanced with decreasing temperature. The S-shape MCD signals are observed for both the sharp absorption line and broad absorption band.

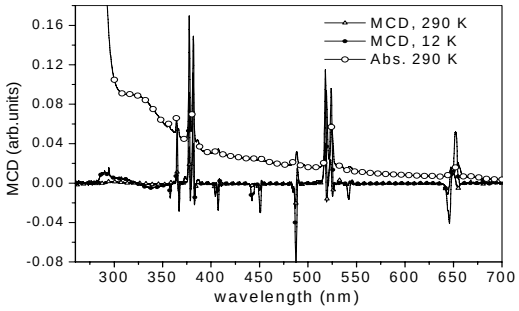


*Fig. 7 MCD and absorption spectra of Er:CNGG. Magnetic field applied for the MCD measurement was 11 kG.*

## 4. Discussion

### 4.1 The temperature-dependent green emission bands

Strongly temperature-dependent emission spectra were observed for the green emission bands as shown in Fig. 5, i.e., the intensities of the emission bands at 540-565 nm increase with decreasing temperature from 290 K, while those of the emission bands at 515-538 nm decrease. In Fig. 8, the intensities of the 522 and 543 nm bands are plotted against temperature. The 522 and 543 nm emission bands are due to the transitions from the $^2H_{11/2}$ and $^4S_{3/2}$ states, respectively.

To explain this temperature dependence, we make a calculation using a two-level model of the $^2H_{11/2}$ and $^4S_{3/2}$ states and non-radiative one-phonon relaxation process between these two states (see inset of Fig. 8). Rate equations are given by

$$\frac{dN_2}{dt} = -k_{21}N_2 - k_2N_2 + k_{12}N_1$$

$$\frac{dN_1}{dt} = +k_{12}N_2 - k_{12}N_1 - k_1N_1$$

$$k_{12} = \frac{1}{e^{E/kT} - 1} * K$$

$$k_{21} = (\frac{1}{e^{E/kT} - 1} + 1) * K$$

where $N_2$ , $N_1$ , $k_2$ and $k_1$ are the populations and the

radiative constants of the levels $^2H_{11/2}$ and $^4S_{3/2}$, respectively. K is the coupling constant between those two levels and E is the energy difference between levels. The initial conditions are assumed as $N_2(t=0)=1$ and $N_1(t=0)=0$.

We neglected the non-radiative transition from the $^4S_{3/2}$ state to the lower-lying $^4F_{9/2}$ state because the gap energy is about 3100 $cm^{-1}$ that does not allow the multi-phonon relaxation by the gap law. Photoluminescence lifetime of the $^4S_{3/2} \rightarrow {}^4I_{15/2}$ transition has two components in $Er^{3+}$-doped CNGG, i.e., a fast decay component of 15.1 μs and the slow component of 30.5 μs [2]. Therefore we use the inverse of 15.1 μs as $k_1$. The energy gap between the $^2H_{11/2}$ and $^4S_{3/2}$ levels were estimated as 675 $cm^{-1}$ at 12 K from the absorption spectra and we use this value as E. Good fitting was obtained between the measured and calculated PL intensities of the two emission bands by choosing values of $k_1=6.25x10^4$ $s^{-1}$, $k_2=1.4x10^5$ $s^{-1}$, $K=12x10^7$ $s^{-1}$, as shown by solid lines in Fig. 8. The radiative lifetime of 0.7 μs estimated for the $^2H_{11/2}$ state is reasonable because it is much shorter than the lifetime of the forbidden $^4S_{3/2}$ state. From this result, we confirm that the thermal activation from the lower $^4S_{3/2}$ state to the $^2H_{11/2}$ state induces the emission from the upper $^2H_{11/2}$ state at high temperatures like 290 K.

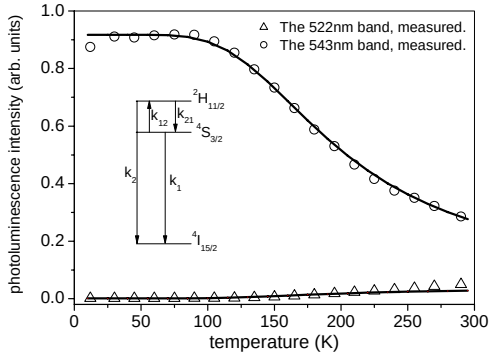


*Fig. 8 Temperature dependence of the 522 and 543 nm emission bands of Er:CNGG crystal. Solid lines are obtained by calculation.*

### 4.2. Near-infrared emissions

Of the near infrared emission bands, only the 860 and 1240 nm bands are not generated by excitation into the 667 nm absorption band (Fig. 2). The 667 nm absorption is due to the $^4I_{15/2} \rightarrow {}^4F_{9/2}$ transition. Therefore the 860 and 1240 nm bands are assigned to the transitions from the $^4S_{3/2}$ state, which locates above the $^4F_{9/2}$ state, to the $^4I_{13/2}$ and $^4I_{11/2}$ states, respectively.

Like the 543 nm emission band due to the transition from the $^4S_{3/2}$ state, the 1240 and 860 nm bands grow with decreasing temperature. This indicates that the above-mentioned assignment to the 1240 and 860 nm emission bands are reasonable.

### 4.3. Ultraviolet broad bands

A broad absorption band is observed at 325 nm. Excitation into this band gives rise to the sharp emissions of $Er^{3+}$ ions. The first parity-allowed absorption band due to the 4f-5d transition in $Er^{3+}$ appear at around 160 nm [11]. Therefore we cannot attribute the 325 nm band to the 4f-5d transition.

Similar broad absorption band is observed near the band-to-band absorption edge in several $Er^{3+}$-doped materials. For example, Dorenbos et al. found a broad band at 283 nm in $LaBr_3$ [3], and the excitation into this band gives sharp $Er^{3+}$ lines. They attributed this band to the charge-transfer (CT) band, where electron is transferred to $Er^{3+}$ from the top of valence band, leaving hole in the valence band of $LaB_3$. Taking into this results, it is suggested that the 325 nm absorption band of CNGG is attributable to the CT band.

The 278 nm absorption band was found by the excitation spectrum for the 470 nm broad emission band. The 278 nm band is close to the band gap of CNGG.. Dorenbos et al. observed absorption band at 250 nm and broad emission band at 393 nm by excitation into the 250 nm band in Er:$LaBr_3$ [3]. Therefore, taking into account the MCD signal of the 278 nm band, it is suggested that the 278 nm band is attributable to a trapped center which is formed by oxygen vacancy in disordered CNGG.

## 5. Summary

Broad emission bands due to $Er^{3+}$ are certainly observed in both the visible and infrared regions because of disordered host crystal of CNGG. Additionally $Er^{3+}$-doped CNGG crystal presents several different characteristics in the emission spectra when compared with other $Er^{3+}$-doped crystals and glasses, especially the near infrared photoluminescence. For example, two emission bands are clearly observed at 860 and 1240 nm

besides the well-known $Er^{3+}$ bands at 1535 nm and at around 1000 nm. The 860 and 1240 nm bands are attributed to the transitions from the same $^4S_{3/2}$ state to the $^4I_{13/2}$ and $^4I_{11/2}$ excited states. The temperature-sensitive behaviour in the green emission bands is explained by non-radiative relaxation processes between the $^2H_{11/2}$ and $^4S_{3/2}$ states. It is suggested that the 325 nm broad absorption band, which gives a board 470 nm emission band, is attributable to the CT band, while another broad 278 nm absorption band to trapped center which is formed by oxygen vacancy in disordered CNGG.

## References

[1] E. V. D. van Loef, P. Dorenbos, C. W. E. van Eijk, K. W. Kramer, H. U. Gudel, Phys. Rev. B **68**, 045108 (2003).

[2] T. Tsuboi, K. Shimamura, T. Fukuda, Phys. Stat. Sol. (b) **214**, 479 (1999).

[3] P. Dorenbos, E. V. D. van Loef, A. P. Vink, E. Van der Kolk, C. W. E. van Eijk, K. W. Kramer, H. U. Gudel, W. M. Higgins, K. S. Shah, J. Lumin. **117**, 147 (2006).

[4] S. Shionoya, W. M. Yen, Phosphor Handbook, CRC Press New York, 1998.

[5] F. Gan, Y. H. Chen, Opt. Mat. **2**, 45 (1993).

[6] Y. F. Ruan, X. M. Wang, T. Tsuboi, J. Alloys and Comp. **275/277**, 246 (1998).

[7] K. Shimamura, K. Timosheckin, T. Sasari, K. Hoshikawa, T. Fukuda, J. Cryst. Growth **128**, 1021 (1993)

[8] Y. Ono, K. Shimamura, Y. Morii, T. Fukuda, T. Kajitani, Physica B, **213/214**, 420 (1995).

[9] K. Shimamura, P. Becker, B. Wyncke, F. Brehat, T. Fukuda, C. Carabatos-Nedelec, J. Phys.: Condens. Matt. **10**, 6865 (1998).

[10] R. Balda, J. Fernandez, M. A. Illaramendi, Phys. Rev. B **48**, 9279 (1993).

[11] P. Dorenbos, J. Lumin. **91**, 91 (2000).

*Corresponding author: silv@infim.ro